PROBING ELECTRIC FIELDS WITHIN ATOMS IN QUANTUM SUPERPOSITION STATES

ONG MING KHAI

XIAMEN UNIVERSITY MALAYSIA

2024

XIAMEN UNIVERSITY MALAYSIA

厦門大學馬來西亞分校

THESIS OF DEGREE

PROBING ELECTRIC FIELDS WITHIN ATOMS IN QUANTUM SUPERPOSITION STATES

NAME OF STUDENT : ONG MING KHAI

STUDENT ID : PHY2009686

SCHOOL/FACULTY : SCHOOL OF MATHEMATICS & PHYSICS

PROGRAMME : BACHELOR OF SCIENCE (HONS.) IN PHYSICS

INTAKE : 2020/09

SUPERVISOR : TOMASZ PATEREK
PROFESSOR

SUPERVISOR : LIM YEN KHENG
ASSOCIATE PROFESSOR

21 JUNE 2024

DECLARATION

I hereby declare that this project report/thesis is based on my original work except for citations and quotations which have been duly acknowledged. I also declare that it has not been previously and concurrently submitted for any other degree or award at Xiamen University Malaysia or other institutions.

Signature : 

Name : Ong Ming Khai

ID No. : PHY2009686

Date : 21/06/2024

APPROVAL FOR SUBMISSION

I certify that this project report/thesis entitled "**PROBING ELECTRIC FIELDS WITHIN ATOMS IN QUANTUM SUPERPOSITION STATES**" that was prepared by ONG MING KHAI has met the required standard for submission in partial fulfilment of the requirements for the award of Bachelor of Science (Hon.) in Physics at Xiamen University Malaysia.

Approved by,

Signature :

Supervisor : Professor Tomasz Paterek

Date :

Signature :

Supervisor : Associate Professor Lim Yen Kheng

Date :

ACKNOWLEDGEMENTS

I would like to express my deepest gratitude to my research supervisors, Prof. Dr. Tomasz Paterek, and Prof. Dr. Lim Yen Kheng, for their invaluable guidance, insights, and immense patience over the course of this project. I would also like to extend my thanks to everyone who contributed to the successful completion of this thesis, especially my family.

ABSTRACT

Quantum gravity is the last obstacle in the way of a Grand Unified Theory. Due to the weak nature of the gravitational force and that larger objects undergo larger decoherence, quantum gravity has not been studied directly. This thesis aims to provide an analogue for a possible experiment by studying the electric field generated by an atom in quantum superposition, drawing from formal analogies between the gravitational and electric force, as well as an idea of what results future experiments using this set-up might obtain.

TABLE OF CONTENTS

DECLARATION ii
APPROVAL FOR SUBMISSION iii
ACKNOWLEDGEMENTS vi
ABSTRACT vii
TABLE OF CONTENTS viii
LIST OF TABLES x
LIST OF FIGURES xi

CHAPTER

1. INTRODUCTION **1**
1.1.Background 1
1.2.Literature Review 1
2. METHODOLOGY **4**
2.1.The Main Idea 4
2.2.Establishing Relevant Transitions 5
2.3.Approach 1: A Hilbert Space Description 7
2.4.Approach 2: A Semi-Classical Approach 13
3. RESULTS **14**
3.1.Average Electric Field Results 14
3.1.1 Fixed Timestep, Range of Impact Parameter 17
3.1.2 Fixed Impact Parameter, Range of Timestep 14
3.2.3.2 Time-Dependent Electric Field Results 19
3.2.1 Fixed Timestep, Range of Impact Parameter 19
3.2.2 Fixed Impact Parameter, Range of Timestep 20
4. DISCUSSION **22**
5. CONCLUSION **22**
REFERENCES **25**

LIST OF FIGURES

Figure 2.1.1:	Diagram of the main idea	4
Figure 2.3.1:	Radial wave functions	9
Figure 2.3.2:	Electric field of target atom	9
Figure 2.3.3:	Model of projectile travelling through electron cloud	10
Figure 3.1.1.1:	Excitation probability of lithium	15
Figure 3.1.1.2:	Excitation probability of hydrogen and potassium	15
Figure 3.1.1.3:	Excitation probability of rubidium	16
Figure 3.1.1.4:	Excitation probability of sodium	16
Figure 3.1.1.5:	Excitation probability of caesium and francium	17
Figure 3.1.2.1:	Excitation probability of lithium	17
Figure 3.1.2.2:	Excitation probability of other atoms	17
Figure 3.2.1.1:	Excitation probability of target atoms	19
Figure 3.2.2.1:	Excitation probability of lithium	20
Figure 3.2.2.2:	Excitation probability of other atoms	20

LIST OF TABLES

Table 2.2.1:	Transition energy data from NIST	6
Table 2.2.2:	Transition frequencies of selected transitions by element	6

CHAPTER 1

INTRODUCTION

1.1 Background

The research described in this thesis is motivated by the questions in the theory of quantum gravity, which presents itself as one of the more prominent unresolved problems in modern physics. It refers to the last missing puzzle piece in the Standard Model: a description of gravitational physics using the principles of quantum mechanics. It would apply primarily to environments and situations where the physics of neither regime can be ignored, such as in the spaces within close proximity to black holes and highly compact astrophysical objects, and the primordial universe before rapid expansion would take place. The basic issue studied in this thesis is how one would describe the gravity of a massive object in spatial quantum superposition.

1.2 Literature Review

Currently, there exist no direct experiments on such gravitational configurations on account of two contradictory demands: (i) gravity is an inherently weak force, and thus necessitates the usage of particles of considerable mass and size to impart a significant gravitational field, and (ii) large objects experience large decoherence, making the preservation of quantum superpositions difficult. Hence, the focus on gravitational fields here is substituted for the simulation and study of electric fields inside atoms prepared in quantum superposition states.

The main reason for this is that the electric force is several orders of magnitude stronger than the gravitational force, which makes the predictions within this thesis that are closer to that which can be tested in laboratories. Furthermore, under gravito-electromagnetism, the Einstein's equations in the regime of weak gravitational fields can be linearized to equations analogous to those of Maxwell's, bringing a direct connection between the electric regime and the gravitational regime (Clark & Tucker, 2000).

The thesis proposes an experiment where a projectile neutral atom is shot towards target atoms, which are prepared in suitable and relatively simple conditions to study

superposition states. As such, the proposed setup is reminiscent of scattering experiments. However, as opposed to conventional scattering experiments, there is less interest in the detailed trajectory of the projectile or statistics of deflections, and the state of target atom is itself very exotic. The figure of merit in this thesis is the probability that the projectile gets excited. The core idea is that this probability will be different across the various approaches in describing the field of the superposed electrons in the atom. There are at least three approaches to do this, which will now be briefly reviewed and later expanded upon in the thesis.

In the first approach, the field generated by the electrons is treated as a separate degree of freedom, and hence in quantum formalism it is described by its own Hilbert space. For gravity, this approach dates back to the thought experiment proposed by Richard Feynman in the 1957 Chapel Hill seminar (Marletto & Vedral, 2017) and has also been explicitly used in calculations of gravitational entanglement by Marletto & Vedral (2017b) and Bose et al. (2017). Accordingly, in the electric-field analogue, one describes an electron and its field by the state in two Hilbert spaces: $|\text{electron}\rangle|\text{field}\rangle$, where the first space describes the electronic configuration (ignoring spin), and the second space describes the electric field. If the electron is superposed across different orbitals, the corresponding electron-field state is assumed to be $|\text{electron 1}\rangle|\text{field 1}\rangle + |\text{electron 2}\rangle|\text{field 2}\rangle$, where the first kets represent the two spatial configurations of the electron, and for the second kets, the field generated when the electron is in the corresponding configuration. If the projectile is now moving through a region of such superposition, it interacts only with the field (all interactions are through the field) and it is shown in the thesis that the state of the field alone is a mixed and time independent state. For slowly moving projectiles, the probability of exciting them is negligible.

In the second approach, the so-called *semi-classical approach*, the field generated by the quantum superposition is calculated by assuming that charge density is proportional to the quantum probability of finding the particle in a given point in space. For gravity, such assumptions appeared in the Schrodinger-Newton model (Bassi et al., 2017), and for electrodynamics they have been thoroughly investigated by Jaynes (1978). From the present proposal's point of view, the superpositions considered are not the eigenstates of the target atoms, and hence they evolve in time. Accordingly, the charge distribution changes in time, leading to the time-dependent electric and

magnetic fields that are computed from the usual Maxwell equations. Changes in the charge density are proportional to the quantum probability of locating the electron around a given point, while the current density is proportional to the quantum probability current. When a projectile propagates through a region of superposition, it experiences time dependent fields and hence the intuition is that the probability of excitation grows as compared with the first approach. This is indeed confirmed by calculations performed later in this thesis. In this way, one can experimentally verify which of the approaches is not correct.

Finally, this thesis will also briefly mention a third approach, which is not something that will be focused on. One could also run this experiment through the machinery of quantum electrodynamics via a field-theoretical approach and compute the probability of excitation in this model. While one would expect the outcomes of such an approach to be closest to real experiments, this approach is beyond the scope of present thesis. The main goal of this thesis is to provide theoretical evidence that the probability of excitation of the projectile can be distinguished between the first two approaches.

CHAPTER 2

METHODOLOGY

2.1 The Main Idea

The main idea of this thesis can be represented by Figure 2.1.1.

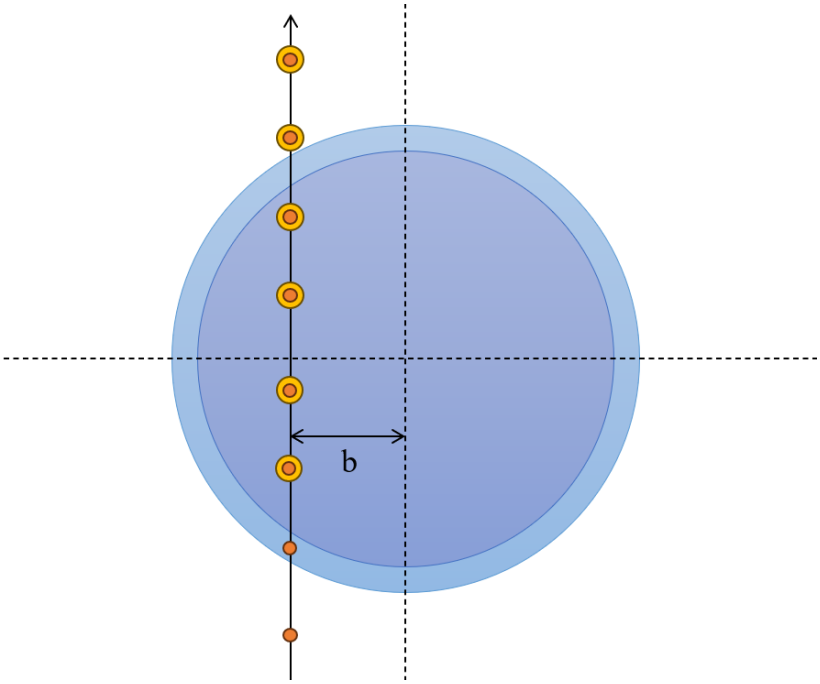

Figure 2.1.1 A hydrogen projectile atom (H) travels through the electron cloud of the larger target atom (blue circles), with impact parameter *b*. We compute the probability to excite the projectile atom and show that it is different in different approaches to describe the field generated by the cloud.

A neutral target atom is prepared in a state of superposition between two orbital energy levels. In the interest of simplifying matters, we set these two states to be s-orbitals of alkali metals, as they have no orbital angular momentum and are hence spherically symmetric. Selecting alkali metals allows us to focus on their single outermost valence electron, while assuming the rest of the atomic structure to be effectively replaced by a $+e$ particle at the centre of the atom. The resulting configuration is a hydrogen-like system, with the superposition involving the electron taking on different principal quantum numbers n, but maintaining $l = 0$ and $m = 0$.

Here, we encounter an issue. This s-orbital to s-orbital transition is dipole forbidden, which raises questions about how exactly such a configuration could be prepared in the target atom. We note that this can be achieved with a Raman configuration of two lasers, which drive the transitions between the s-orbitals and an additional intermediate state for which the dipole transition is allowed.

Another neutral atom is prepared to serve as a projectile, propagating through the electron cloud of the target atom. For simplicity, we assume that the path of this projectile atom is a straight line, i.e. the electric field of the target atom is approximately uniform across the wave function of the projectile such that no net force acts on the projectile. In such a case, it is also plausible to invoke dipole approximation and treat the projectile's internal electronic configuration as a two-level system, involving energy levels that closely match the possible oscillations in the field of the target atoms. The thesis will go into further detail on the steps executed, but we found it appropriate to clarify the physical assumptions made before doing so.

2.2 Establishing Relevant Transitions

In order to ensure our setup is physically plausible, we must first determine the species of the target and projectile atoms, and check if there exists a transition between energy levels in the projectile atom that has a frequency comparable to the energy difference between the superposed states in the target atom, which, in the semi-classical approach, would be the frequency of the oscillating field.

The hydrogen atom is selected to serve as the probe in this setup, primarily due to its simplicity. However, we note that the probe cannot be prepared in its ground state, as exciting it to a higher energy level from the ground state requires more energy than any difference of energy states of the heavier atom, exceeding even their ionization energies, assuming the absence of external electric and/or magnetic fields. Hence, we opt to use the 2s to 3p transition, which is dipole allowed and incurs a less expensive energy cost of 1.889eV. The 2s state of hydrogen is also meta-stable state for its electron to occupy with a lifetime of 0.12 seconds. The probe atom is expected to complete its trajectory within a time frame on the order of femtoseconds, so we are not concerned with the spontaneous emission of the hydrogen projectile to the ground state.

With this probe atom transition in mind, we select target alkali metals transitions with energies closely matching the 2s to 3p orbital transition.

Source Atom	Lower State	Upper State	Lower eV	Upper eV	Transition Energy (eV)
H	2s	4s	10.199	12.749	2.550
Li	3s	11s	3.373	5.271	1.897
Na	4s	17s	3.191	5.084	1.892
K	4s	5s	0	2.607	2.607
Rb	5s	6s	0	2.496	2.496
Cs	6s	7s	0	2.298	2.298
Fr	7s	8s	0	2.447	2.447

Table 2.2.1 Transition energy data from NIST

Table 2.1 organizes values derived from the NIST database of energy levels and transitions. It should be noted that a closer match to the probe atom transition is obtained for lithium and sodium, where the transition is between the first excited state and a much higher Rydberg state. Conversely, for heavier elements, the match is less accurate, with transitions between the ground state and first excited state for heavier elements. This is because, as far as the NIST is concerned, there exist no other transitions for these heavier elements that can overcome the 2s to 3p energy requirement.

With our table of accepted transitions, we can convert the transition energies into transition frequencies that will be relevant for upcoming calculations:

$$E = hf = \frac{\omega h}{2\pi},$$

$$\omega = \frac{2\pi \cdot E}{h} = \frac{1.602 \times 10^{-19} E[\text{eV}]}{\hbar}.$$

We may obtain the following table relevant for upcoming calculations.

Source Atom	Transition Frequency ω (in petahertz PHz)
H	3.874
Li	2.883
Na	2.874
K	3.961
Rb	3.792
Cs	3.491
Fr	3.718

Table 2.2.2 Transition frequencies of selected transitions by element

As this projectile atom, or probe atom, travels through the electron cloud, it is subjected to different magnitudes of electric fields. Hence, even when the field is static in time, its charge variations in space are perceived by the projectile atom as a time dependent field and accordingly there is a chance of excitation even in this case.

2.3 Approach 1: A Hilbert Space Description

In the first approach, we will assume that the target atom and field state are described by:

$$|ns\rangle|E_n\rangle + |ms\rangle|E_m\rangle, \tag{2.3.1}$$

where $|E_n\rangle$ is the state describing the electric field generated by the electron in the orbital $|\mathrm{ns}\rangle$, and similarly for $|E_m\rangle$ and $|ms\rangle$ for the second term in the sum. The states $|ns\rangle$ are stationary and acquire the phase $e^{-\frac{it}{\hbar}E_n}$ over time, where E_n is the corresponding energy eigenvalue. Hence, the state described in (1) evolving in time reads:

$$e^{-\frac{it}{\hbar}E_n}|ns\rangle|E_n\rangle + e^{-\frac{it}{\hbar}E_m}|ms\rangle|E_m\rangle. \tag{2.3.2}$$

Since the orbitals $|\mathrm{ns}\rangle$ are orthogonal, the state of the field on its own is given as:

$$\rho_E = \frac{1}{2}|E_n\rangle\langle E_n| + \frac{1}{2}|E_m\rangle\langle E_m|. \tag{2.3.3}$$

Therefore, the probe atom interacts with the field in this mixed state $\frac{1}{2}|E_n\rangle\langle E_n| + \frac{1}{2}|E_m\rangle\langle E_m|$, which is time independent. The field experienced by the projectile is the average of the electric fields from the $|ns\rangle$ and $|ms\rangle$ orbitals. We will now calculate this field.

We begin by considering the outermost electron in a single s-orbital of the target atom. Since these orbitals are spherically symmetric, we may obtain the electric field via an application of the Gauss Law:

$$\rho(\vec{r}) = +e\delta(\vec{r}) - e|\psi(\vec{r})|^2, \tag{2.3.4}$$

$$E(r) = \frac{1}{4\pi\epsilon_0 r^2}\int_0^r \rho(\overrightarrow{r'})d\overrightarrow{r'}$$

$$= \frac{1}{\epsilon_0 r^2} \int_0^r \rho(r')\, r'^2 d\vec{r'}\,. \tag{2.3.5}$$

Where $\rho(\vec{r'})$ refers to the total charge distribution, with two terms describing the core of the target atom and the electron cloud of its s-orbital (assuming it was given by $-e|\psi(\vec{r'})|^2$), while $E(r)$ is the resulting electric field at radial distance r from the origin. Thanks to symmetry, they are both functions of radial distance only. The full wave functions of hydrogenic orbitals are given by:

$$\psi_{n,l,m}(\vec{r}) = R_{n,l}(r) Y_{l,m}(\theta, \phi). \tag{2.3.6}$$

For the s-orbitals, the spherical harmonic component $Y_{l,m}$ is defined by a simple constant $Y_{0,0} = \frac{1}{2\sqrt{\pi}}$. The radial wave function $R_{n,l}(r)$ at higher levels is not explicitly given in existing literature, and therefore we have developed a Python script to generate wavefunctions based on defined *n*, *l*, and *m* values. The script utilizes the following relations that are known for describing the radial wave functions:

$$R(\rho) = \rho^l \sum_{k=0}^{n-l-1} \alpha_k\, \rho^k e^{-\frac{\rho}{2}}, \tag{2.3.7}$$

$$\rho = \frac{2Z}{n\alpha_0} r, \tag{2.3.8}$$

$$\alpha_{k+1} = \alpha_k \frac{k + l + 1 - n}{(k+1)(k+2l+2)}. \tag{2.3.9}$$

Here, Z denotes the atomic number, or number of protons in the atom, however within this value has been set to 1 throughout all simulations in this thesis. Since we are considering both the nucleus and the inner electrons of the target atom to be a single point in the centre with a $+e$ charge, it is functionally identical to a Z=1 hydrogen atom and treated as such. It should be mentioned that the Python script also normalizes the computed radial wavefunction before returning the requested values of ψ. The final results were thoroughly checked with existing data for lower excited states to verify their accuracy. Figure 2.3.1 shows the radial functions for small as well as larger values of n.

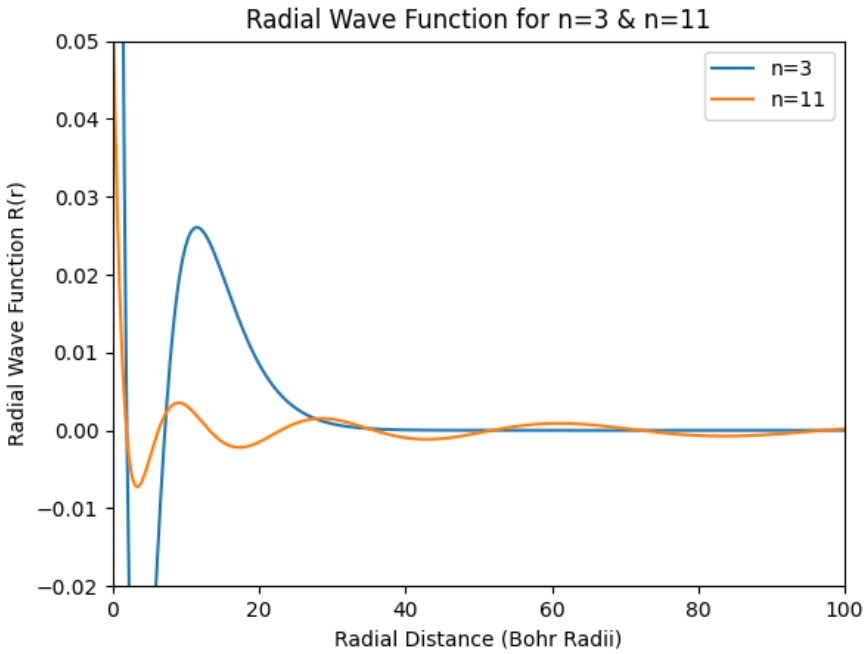

Figure 2.3.1 Radial wave functions for n =3 and n =11 s-orbitals (l=0)

Given concrete values of the radial wave functions, we are able to compute ρ and finally $E(r)$. Figure 2.3.2 shows the resulting field for the example of a lithium target superposed between the 3s and 11s orbitals.

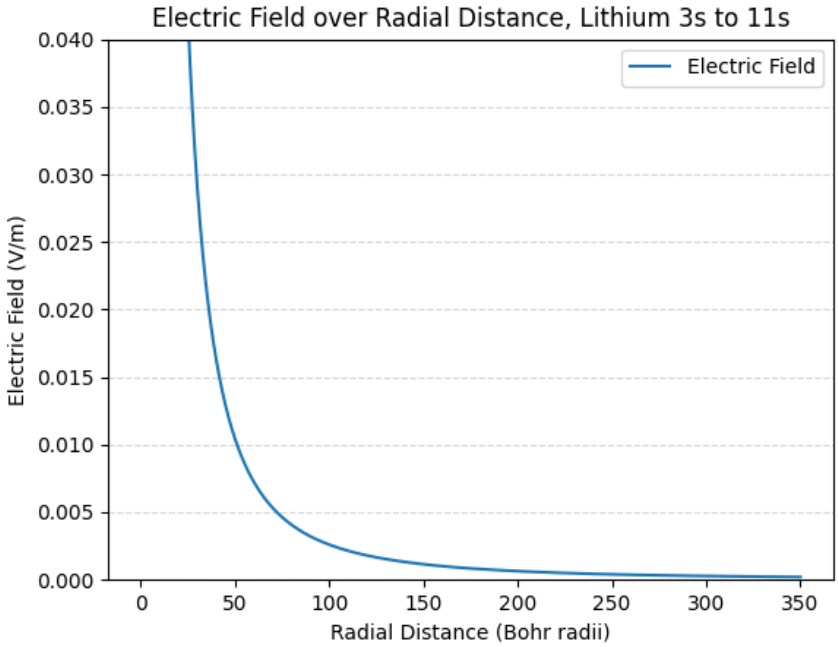

Figure 2.3.2 Electric field of a lithium target atom (3s to 11s transition)

The next step is to evaluate the field experienced by the probe atom. Its trajectory is set to be a straight path off-centre relative to the centre of the target atom, with a defined closest approach *b* that will be varied in the simulations.

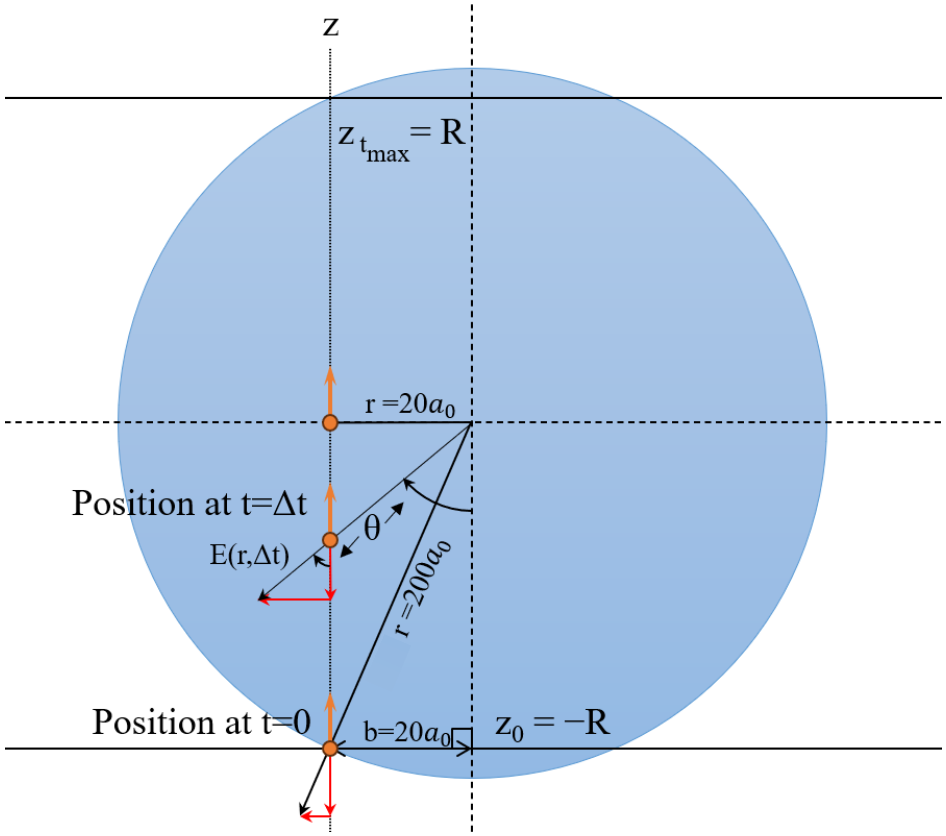

Figure 2.3.3 Model of the projectile travelling through the electron cloud

In the above example, we set the radius of the electron cloud within which the dynamics of the model are calculated to $R = 200a_0$, where a_0 denotes the Bohr radius. This is because after a certain radial distance, the magnitude of the electric field there becomes inconsequentially small ($E(200a_0)$ verified to be 0.00068 V/m in this example), allowing us to ignore these outlaying regions and focus on the interactions taking place in those with higher field strengths. As seen in Figure 2.3.3, the projectile moves along a straight line through the electron cloud at a constant velocity. This trajectory reads:

$$z(t) = -R + vt \tag{2.3.10}$$

The velocity is a parameter in the simulation, with the projectile always starting at $z(0) = -R$. We also define a final time $t_{max} = \frac{2R}{v}$, such that the simulation is ended

when the projectile reaches $z = R$. The time interval is divided into n steps, where $\Delta t = \frac{t_{max}}{n}$. In order to evaluate the field on the path as seen above, we use the relation:

$$r(t) = \sqrt{b^2 + z(t)^2} \tag{2.3.11}$$

Where $r(t)$ refers to the radial distance of the probe atom relative to the centre of the target atom. It will soon become clear that only the z-component of the field is required, which is seen in Figure 2.3.3 to satisfy:

$$E_z = -\cos\theta\, E(r) = \frac{z(t)}{r(t)} E\big(r(t)\big) \tag{2.3.12}$$

The reason why we attach such focus over the z-component of the electric field lies in the dipole coupling. The dipole would be aligned along the z-axis for the entirety of its journey. In an open system, the electric dipole would interact with the external electric field of the source atom, but in this case, we are operating with a closed system, so the orientation of the dipole will remain unaffected. The dipole moment operator of the probe atom is given by:

$$\mu = \begin{pmatrix} 0 & \mu_{23} \\ \mu_{23}^* & 0 \end{pmatrix} \tag{2.3.13}$$

Where the diagonal elements have vanished due to symmetry of the orbitals, and the off-diagonal term is given by:

$$-e\langle 2s|\vec{r}|3p\rangle$$

The components $\langle 2s|x|3p\rangle$ and $\langle 2s|y|3p\rangle$ equal 0, leaving $\langle 2s|z|3p\rangle$ as the only non-zero term. This gives rise to the off-diagonal term, equal to:

$$\mu_{23} = -e\langle 2s|z|3p\rangle = -e\int \psi_{2s}(\vec{r}) \cdot z \cdot \psi_{3p}(\vec{r}) d\vec{r}$$

$$= -e\int_0^\infty \int_0^\pi \int_0^{2\pi} \psi_{2s}(\vec{r}) \cdot z \cdot \psi_{3p}(\vec{r}) r^2 \sin\theta\, dr d\theta d\phi$$

$$= -e\int_0^\infty R_{2,0}(r\cos\theta) R_{3,1} r^2 dr \int_0^\pi \mathrm{Y}_{0,0}\mathrm{Y}_{1,0} \sin\theta\, d\theta \int_0^{2\pi} d\phi$$

$$= -e\int_0^\infty R_{2,0} R_{3,1} r^3 dr \int_0^\pi \left(\frac{1}{2\sqrt{\pi}}\right)\left(\sqrt{\frac{3}{4\pi}}\cos\theta\right) \cos\theta \sin\theta\, d\theta \int_0^{2\pi} d\phi$$

$$= -e\left(\frac{1024(3)^{\frac{9}{2}}}{15625}a_0\right)\cdot\frac{\sqrt{3}}{4\pi}\left(\frac{2}{3}\right)\cdot 2\pi \cong -e(5.308416) = -5.3084\text{eV} = \delta \quad (2.3.14)$$

This returns the magnitude of the electric dipole moment of the probe atom. We now compute the probe-target interaction from the Hamiltonian:

$$H = H_0 + H_{int}. \quad (2.3.15)$$

Where H_0 describes the energy of the probe in the relevant subspace, and $H_{int} = -\vec{\mu}\cdot\vec{E} = -\mu_{23}E_z$. In the matrix form, we thus have:

$$H = \begin{pmatrix} E_{2s} & -E_z\delta \\ -E_z\delta & E_{3p} \end{pmatrix}. \quad (2.3.16)$$

With eigenvalues of the matrix being:

$$\lambda_{\pm}(t) = E_{\pm}(t) = \frac{1}{2}\left(E_{2s} + E_{3p} \pm \sqrt{\left(E_{2s} - E_{3p}\right)^2 + \left(4E_z^2(t)\delta^2\right)}\right). \quad (2.3.17)$$

Incidentally, the square root term is the so-called *Rabi frequency* of the system, henceforth referred to in a simpler Ω notation. The eigenstates of this Hamiltonian are as follows:

$$|\phi_+(t)\rangle = \sqrt{\frac{\Omega(\mathrm{t}) - \left(E_{2s} - E_{3p}\right)}{2\Omega(\mathrm{t})}}\,|3p\rangle + \sqrt{1 - \frac{\Omega(\mathrm{t}) - \left(E_{2s} - E_{3p}\right)}{2\Omega(\mathrm{t})}}\,|2s\rangle \quad (2.3.18)$$

$$|\phi_+(t)\rangle = \alpha(t)|3p\rangle + \beta(t)|2s\rangle$$

$$|\phi_-(t)\rangle = \beta(t)|3p\rangle - \alpha(t)|2s\rangle$$

The initial state of the dynamical system is the probe atom in the $|2s\rangle$ state. At time zero, the energy eigenstates read:

$$|2s\rangle = \beta(0)|\phi_+(0)\rangle - \alpha(0)|\phi_-(0)\rangle, \quad (2.3.19)$$

and the state of the system being:

$$|\psi_0\rangle = \beta(0)|\phi_+(0)\rangle - \alpha(0)|\phi_-(0)\rangle = \gamma_0|\phi_+(0)\rangle + \delta_0|\phi_-(0)\rangle.$$

At this Δt time, the probe will have moved by Δz along the z-axis, and hence interact with a different electric field. The Hamiltonian now has new eigenvalues and eigenstates because the Rabi frequency has changed to $\Omega(\Delta t)$. We therefore expand the state $|\psi_{\Delta t}\rangle$ in the eigenbasis of the Hamiltonian at time Δt:

$$|\psi_{\Delta t}\rangle = \gamma_0 e^{-\frac{i\Delta t}{\hbar}E_+(0)}|\phi_+(0)\rangle + \delta_0 e^{-\frac{i\Delta t}{\hbar}E_-(0)}\,|\phi_-(0)\rangle,$$

$$|\psi_{\Delta t}\rangle = \gamma_1|\phi_+(\Delta t)\rangle + \delta_1|\phi_-(\Delta t)\rangle,$$

$$\gamma_1 = \langle\phi_+(\Delta t)|\psi_{\Delta t}\rangle, \qquad \delta_1 = \langle\phi_-(\Delta t)|\psi_{\Delta t}\rangle \tag{2.3.21}$$

which evolves to $2\Delta t$ using the eigenvalues at Δt:

$$|\psi_{2\Delta t}\rangle = \gamma_1 e^{-\frac{i\Delta t}{\hbar}E_+(\Delta t)}|\phi_+(\Delta t)\rangle + \delta_1 e^{-\frac{i\Delta t}{\hbar}E_-(\Delta t)}|\phi_-(\Delta t)\rangle,$$

$$|\psi_{2\Delta t}\rangle = \gamma_2|\phi_+(2\Delta t)\rangle + \delta_2|\phi_-(2\Delta t)\rangle,$$

$$\gamma_2 = \langle\phi_+(2\Delta t)|\psi_{2\Delta t}\rangle, \qquad \delta_2 = \langle\phi_-(2\Delta t)|\psi_{2\Delta t}\rangle \tag{2.3.22}$$

We continue this process for n steps Δt. For completeness, we present the formula for the next step of Δt:

$$\left|\psi_{(j+1)\Delta t}\right\rangle = \gamma_j e^{-\frac{i\Delta t}{\hbar}E_+(\mathrm{j}\Delta t)}\,|\phi_+(j\Delta t)\rangle + \delta_j\, e^{-\frac{i\Delta t}{\hbar}E_-(j\Delta t)}\,|\phi_-(j\Delta t)\rangle, \tag{2.3.23}$$

where $\gamma_j = \langle\phi_+(j\Delta t)\left|\psi_{j\Delta t}\right\rangle$ and $\delta_j = \langle\phi_-(j\Delta t)\left|\psi_{j\Delta t}\right\rangle$. This final probability of excitation is given by $\left|\langle 3p\left|\psi_{t_{max}}\right\rangle\right|^2$, which expands to:

$$|3p\rangle = \alpha(t)|\phi_+(t)\rangle + \beta(t)|\phi_-(t)\rangle, \langle 3p| = \alpha(t)\langle\phi_+| + \beta(t)\langle\phi_-|$$

$$|\psi_{t_{max}}\rangle = \gamma_{t_{max}}|\phi_+(t_{max})\rangle + \delta_{t_{max}}|\phi_{-(t_{max})}\rangle$$

$$\begin{aligned}\left|\langle 3p|\psi_{t_{max}}\rangle\right|^2 = |&\alpha_{t_{max}}\gamma_{t_{max}}\langle\phi_+(t_{max})|\phi_+(t_{max})\rangle \\ &+ \beta_{t_{max}}\delta_{t_{max}}\langle\phi_-(t_{max})|\phi_-(t_{max})\rangle|^2\end{aligned}$$

$$P^* = |\langle 3p|\psi(t)\rangle|^2 = \left|\alpha(t_{max})\gamma_{t_{max}} + \beta(t_{max})\delta_{t_{max}}\right|^2 \tag{2.3.24}$$

From here, we calculate the probability of excitation P^*, with a final outcome of $P^*(b)$, where b is the impact parameter.

The program utilizes for-loops to repeatedly evaluate an evolving system at each timestep until the end of the probe atom's journey, in order to obtain the final probability of excitation for a given range of propagation times or impact parameters.

2.4 Approach 2: A Semi-Classical Approach

Similarly to the previous approach, the electric field is obtained from the charge distribution $\rho(r)$, but with the electronic contribution being given by the superposition

$\psi(r) = \frac{1}{\sqrt{2}}(\psi_{3s} + \psi_{11s})$, as an example for a model that uses lithium as the target atom element. The difference here is that in the semi-classical approach, we do not use the average of the electric field of the two states, instead considering the time-dependent oscillation of the target atom, and hence the electric field, between the two states. Accordingly:

$$|\psi(R,t)|^2 = \frac{1}{2}|\psi_a(R,t)|^2 + \frac{1}{2}|\psi_b(R,t)|^2 + \frac{1}{2}(\psi_a\bar{\psi}_b + \bar{\psi}_a\psi_b)$$

$$|\psi(R,t)|^2 = \frac{1}{2}|\psi_a(R,t)|^2 + \frac{1}{2}|\psi_b(R,t)|^2 + \psi_a\psi_b\cos(\omega t) \qquad (2.4.1)$$

In this case ψ becomes a function of both radial distance R and time t, and so does the charge distribution and electric field. It should be noted, however, that the $\cos(\omega t)$ oscillations are only present in the spatial region where the wave functions ψ_{3s} and ψ_{11s} overlap. An advantage of employing a spherically symmetrical setup is that the resulting radial current does not admit a magnetic field, as it is well known that in this case the contribution from the motion of charges cancels out with the displacement current (Feynman et al., 1964).

CHAPTER 3

RESULTS

3.1 Average Electric Field Results

3.1.1 Fixed Impact Parameter, Range of Timestep

We begin with a lithium target atom in superposition between 3s and 11s orbitals. The impact parameter has been fixed to 20 Bohr radii, and the program is instructed to calculate the probability of excitation over a range of timesteps (in that the probe atom takes this amount of time to clear the electron cloud) from 1 to 100 with intervals of 1 femtosecond. Below is the resulting excitation probability graph:

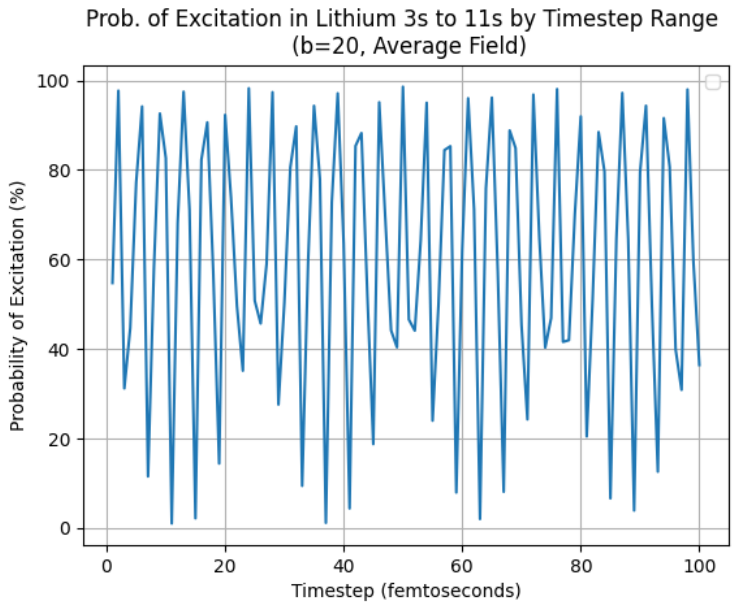

Figure 3.1.1.1 Excitation probability of lithium target atom

We repeat this for other target atom configurations, for which similar results may be obtained:

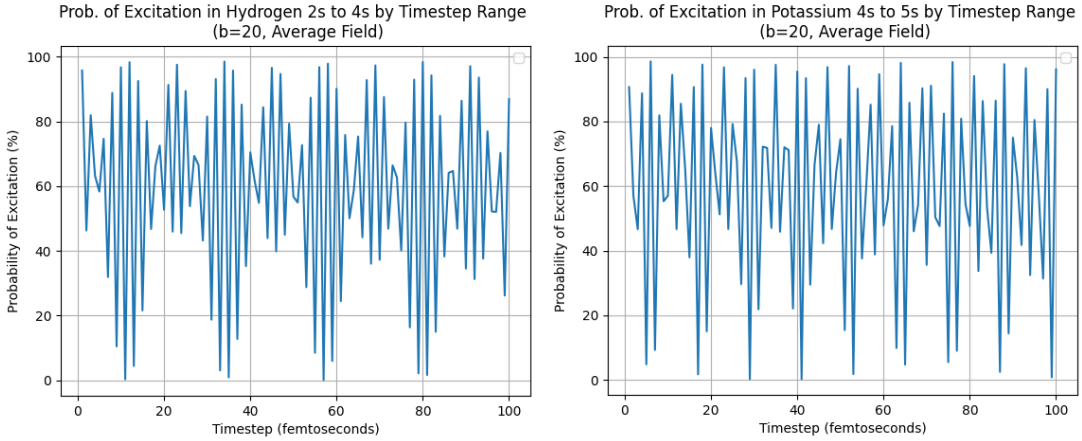

Figure 3.1.1.2 Excitation probability of hydrogen and potassium target atom

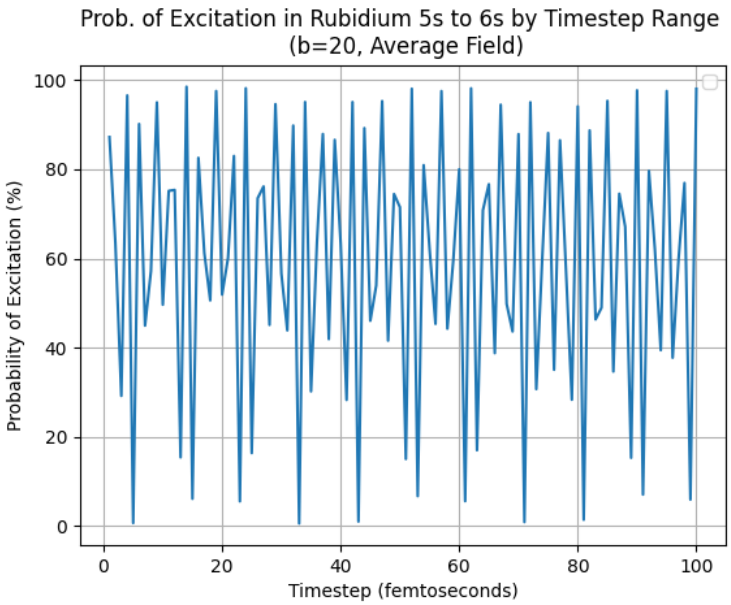

Figure 3.1.1.3 Excitation probability of rubidium target atom

When iterating over a range of timesteps, it becomes apparent that there is a periodicity in the multiple peaks and valleys that are spread out over the range of timesteps. However, the shape of this signal varies between configurations, as seen in the following cases:

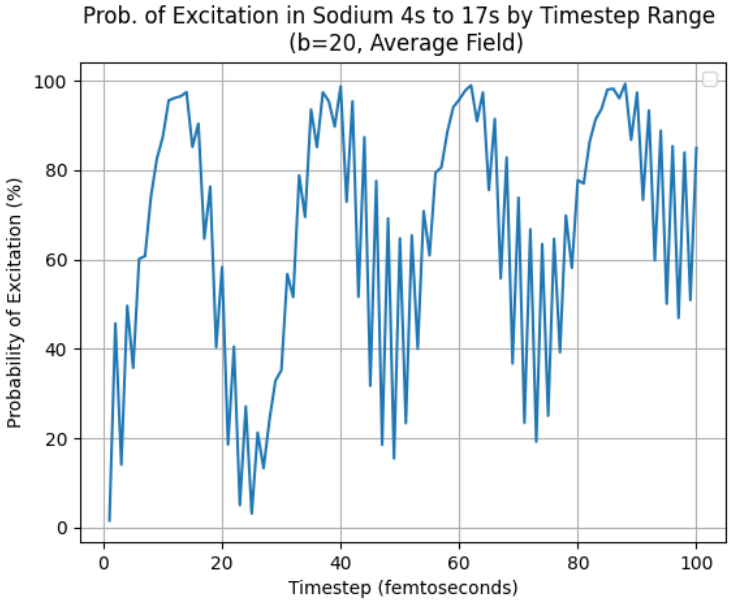

Figure 3.1.1.4 Excitation probability of sodium target atom

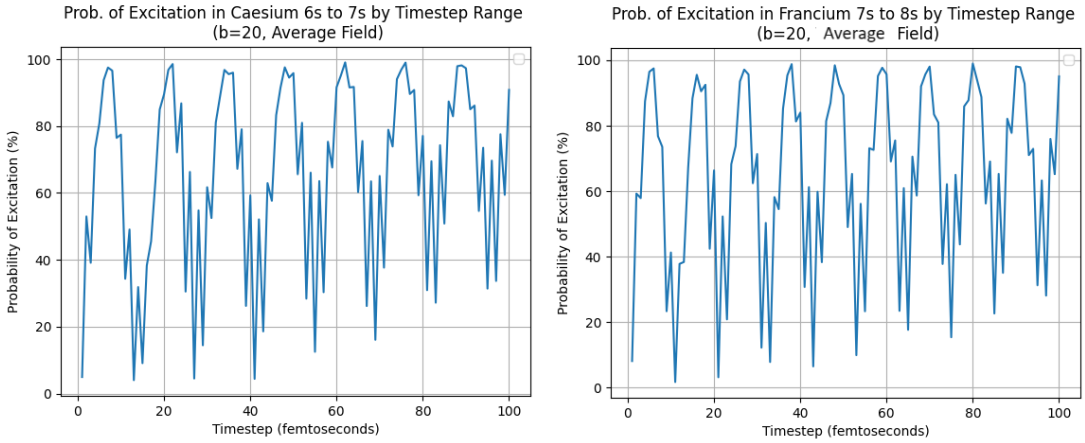

Figure 3.1.1.5 Excitation probability of caesium & francium target atoms

The exact cause for this notable change in signal shape is unclear to us, given that the target atom configurations of sodium, caesium, and francium possess similar parameters of transition energy and frequency to other configurations but do not share similar probabilities of excitation over the timestep range. It is possible that these are simply products of their impact parameters being within a region that favours these excitation probabilities.

3.1.2 Fixed Timestep, Range of Impact Parameter

A change is made to the parameters, in that the timestep is now fixed at a timestep of 20 femtoseconds. The program then iterates over b impact parameters from 0 to 99 Bohr radii with intervals of 1 Bohr radii. Below are a selection of graphs using these parameters:

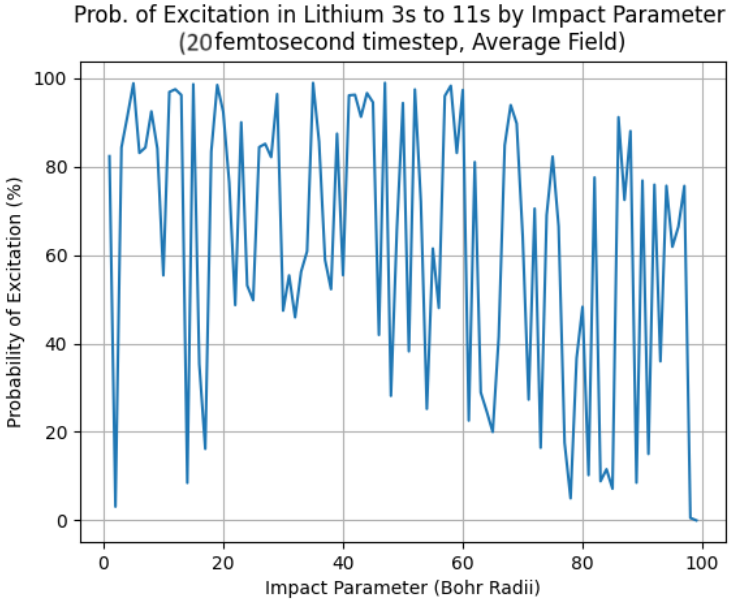

Figure 3.1.2.1 Excitation probability of lithium target atom

We may also compute the probabilities for the other elements of target atoms:

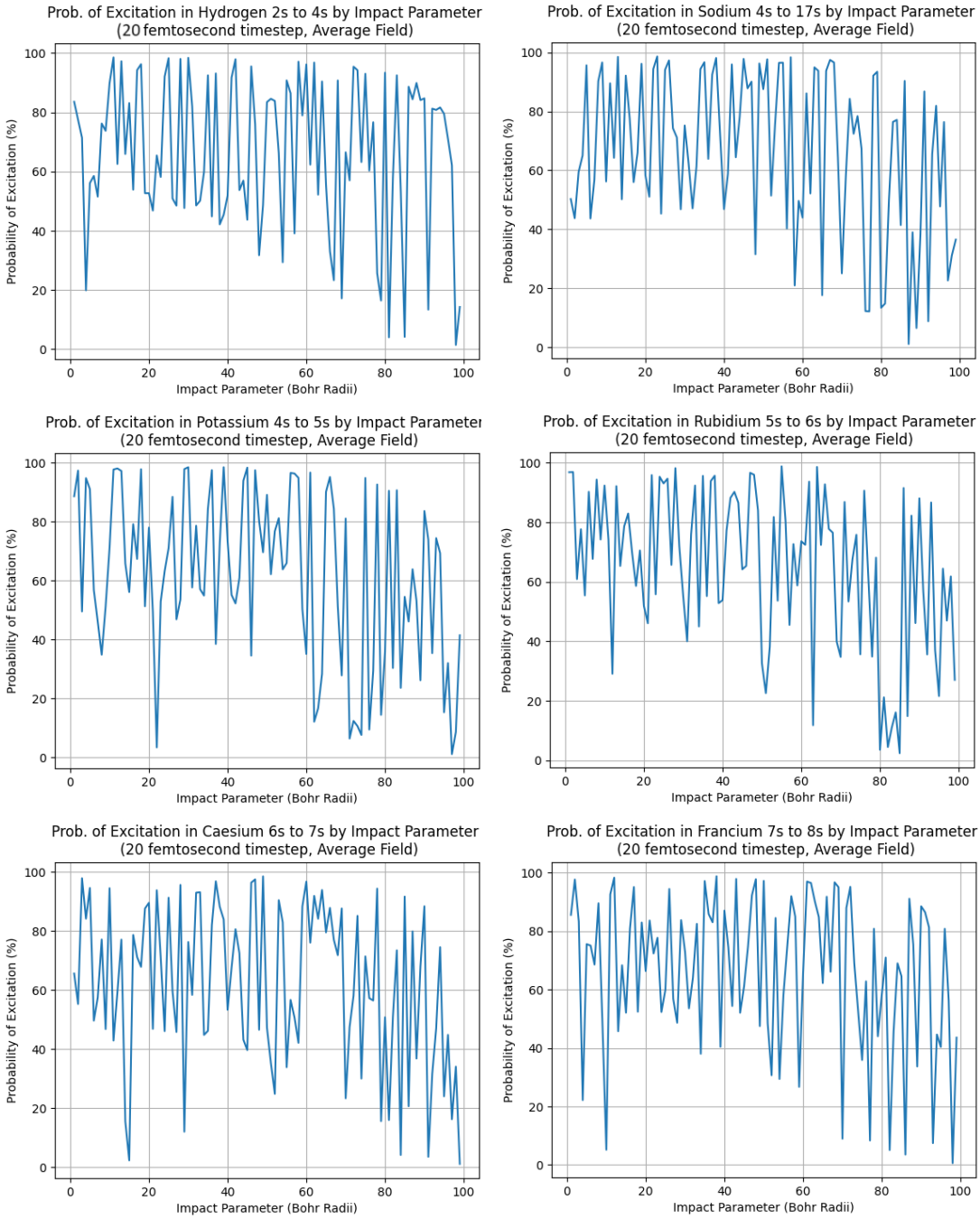

Figure 3.1.2.2 Excitation probability of other target atoms

While we find that there does not seem to be any significant difference between target atom configurations, the minimum probability of excitation appears to increase as the impact parameter increases.

3.2 Time-Dependent Electric Field Results

3.2.1 Fixed Impact Parameter, Range of Timestep

We repeat the above simulations, but use the second approach to obtain the electric field of the target atom.

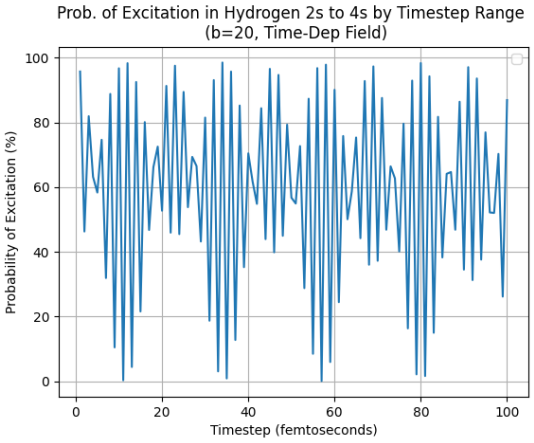

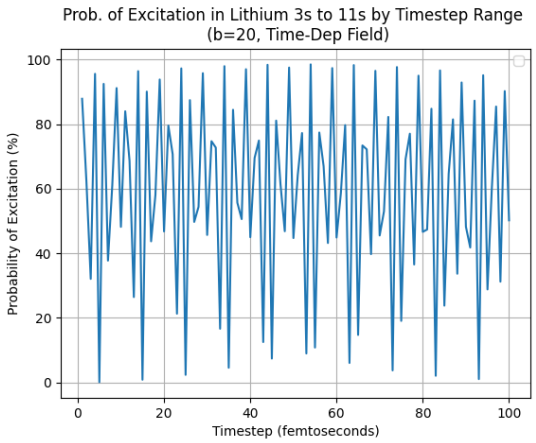

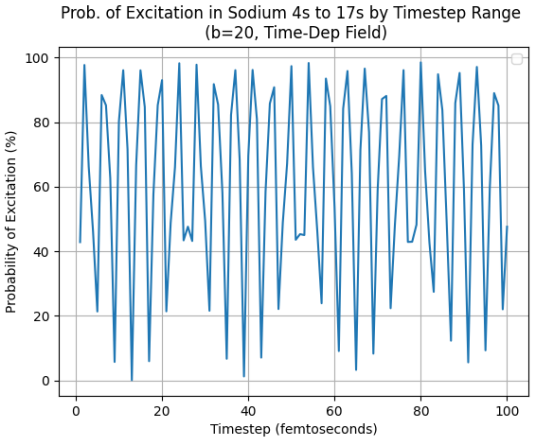

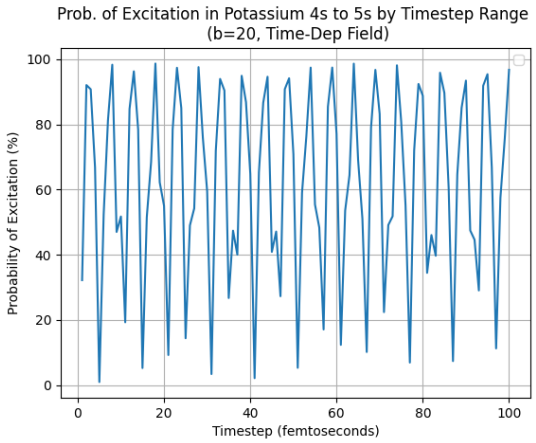

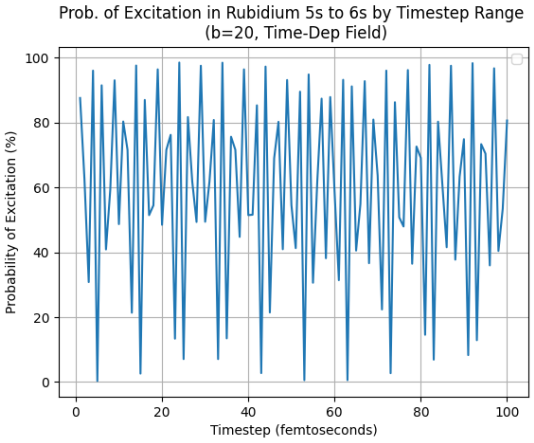

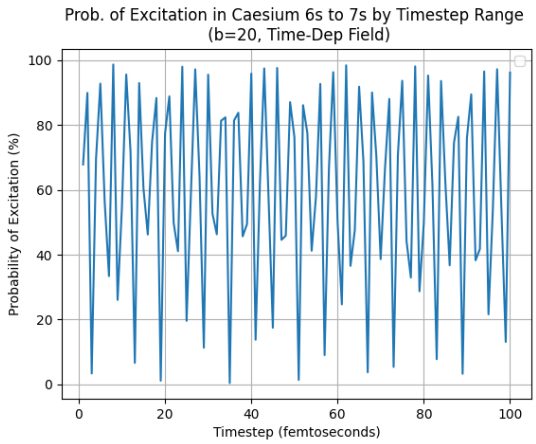

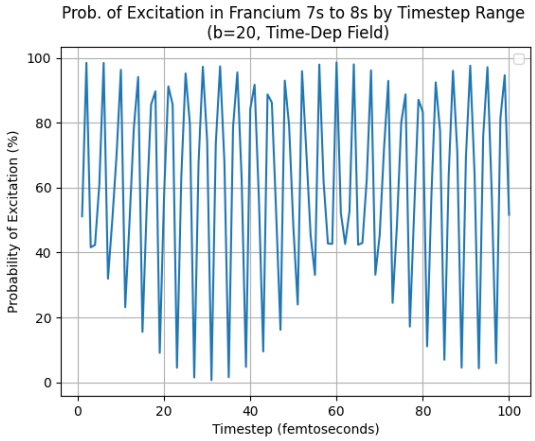

Figure 3.2.1.1 Excitation probability of target atoms

Outside the cases for sodium, caesium, and francium, there does not appear to be any significant difference between the two approaches in the case of a fixed impact parameter and increasing timestep. However, the periodicity of the results become more visible, especially in the case of the francium target atom configuration.

Interestingly, the results for the hydrogen target atom configuration are the exact same in both approaches.

3.2.2 Fixed Timestep, Range of Impact Parameter

Repeating the steps taken in the first approach, the timestep is set to 20 femtoseconds over an increasing range of impact parameters. For the lithium target atom configuration, we obtain:

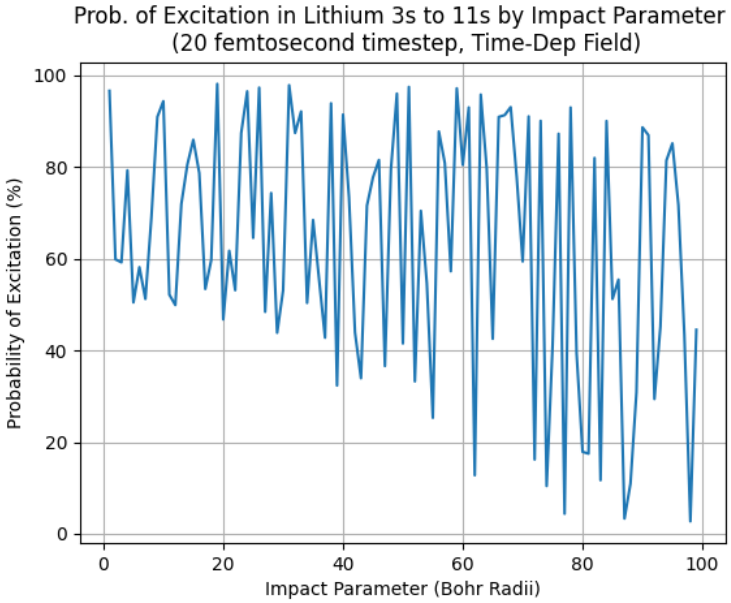

Figure 3.2.2.1 Excitation probability of lithium target atom

It appears that in using the second approach, the excitation probability of the lithium target atom remains higher at certain points even with higher impact parameters, whereas noticeable reductions in this probability may also be observed at sporadic impact parameters.

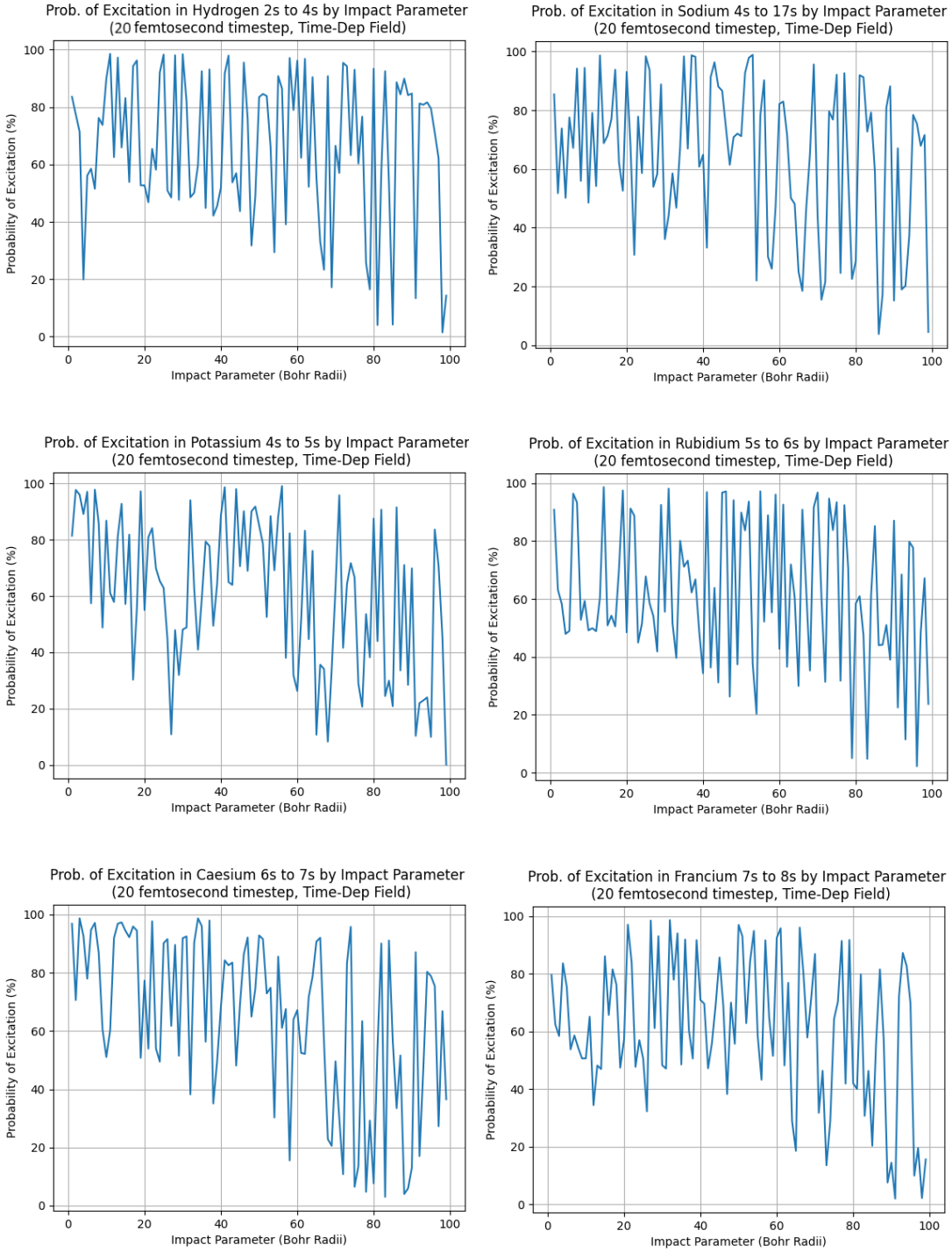

Figure 3.2.2.2 Excitation probability of target atoms

CHAPTER 4

DISCUSSION

These changes in probability arise from the oscillation of the electric field. Depending on the specific impact parameter and timestep, it is possible to significantly increase or decrease the probability of excitation simply by taking note of where and when the electric field of the target atom may increase or decrease relative to its average field.

The model used in this thesis is ultimately tailored towards an analysis of electric forces. If one is to make any statements about quantum gravity, they would need to re-interpret the field of the system as gravitational instead of electric. The target atom, instead of being in a state of quantum superposition between two energy states, would be analogous to a massive thin spherical shell which, depending on the approach used to interpret it, either originates the average gravitational field of a larger and smaller mass (approach 1), or an oscillating gravitational field which implies a mass distribution that changes significantly over time (approach 2). In the simplest analogy, the probe atom would be a similar thin spherical shell that has a non-zero probability of having its mass distribution altered upon exiting the gravitational field of the larger atom.

As mentioned earlier, several assumptions have been made over the course of this thesis to simplify calculations, and it is possible that any physical experiment conducted on this model may diverge from the results obtained in this thesis.

CHAPTER 5

CONCLUSION

We have demonstrated that there is a non-negligible difference between the probability of excitation when calculated for an average field and an oscillating field in the semi-classical method under certain configurations.

We find that the probability of excitation is consistently greater when the impact parameter is small, and the probe atom is allowed to propagate in close proximity to

the centre of the target atom. As the impact parameter increases, the excitation probability decreases, but the rate of this decline is not identical between the two approaches, with the semi-classical approach allowing for higher probabilities at certain points in the lithium target atom configuration, while in other configurations, a lower probability may be obtained instead.

This discrepancy comes from the electric field produced by the target atom, which drives this potential excitation via its z-component. Hence, the distinguishability between approaches is only prevalent when the probe atom has a lower probability of excitation in the average field model to begin with, and even then, the semi-classical method does not necessarily lead to only increases in excitation probability.

It may be possible to more easily distinguish between these two approaches by increasing the strength of the electric field of the target atom, such as by setting its transition to be from the ground state to a much higher n quantum state. This would serve to provide a lower average field, as a high n quantum state would have a charge density spread out over a larger radial distance. Alternatively, increasing the dipole moment of the probe atom by selecting a transition with higher spatial separation would also serve to increase the contrast between excitation probability in the two approaches. However, there is a limit on what probe atom transitions we can use, given that the higher excited states of hydrogen have increasingly shorter lifetimes.

REFERENCES

Bassi, A., Großardt, A., & Ulbricht, H. (2017). Gravitational decoherence. Classical and Quantum Gravity, 34(19), 193002. https://doi.org/10.1088/1361-6382/aa864f

Bose, S., Mazumdar, A., Morley, G. W., Ulbricht, H., Toroš, M., Paternostro, M., Geraci, A. A., Barker, P. F., Kim, M. S., & Milburn, G. (2017). Spin Entanglement Witness for Quantum Gravity. Physical Review Letters, 119(24). https://doi.org/10.1103/physrevlett.119.240401

Clark, S. J., & Tucker, R. W. (2000). Gauge symmetry and gravito-electromagnetism. Classical and Quantum Gravity, 17(19), 4125–4157. https://doi.org/10.1088/0264-9381/17/19/311

Feynman, R. P., Leighton, R. B., Sands, M., & Treiman, S. B. (1964). The Feynman lectures on Physics. *Physics Today, 17*(8), 45–46. https://doi.org/10.1063/1.3051743

Jaynes, E. T. (1978). Electrodynamics Today. In Springer eBooks (pp. 495–509). https://doi.org/10.1007/978-1-4757-0665-9_54

Marletto, C., & Vedral, V. (2017). Witness gravity's quantum side in the lab. Nature, 547(7662), 156–158. https://doi.org/10.1038/547156a

Marletto, C., & Vedral, V. (2017b). Gravitationally Induced Entanglement between Two Massive Particles is Sufficient Evidence of Quantum Effects in Gravity. Physical Review Letters, 119(24). https://doi.org/10.1103/physrevlett.119.240402

NIST: Atomic Spectra Database - Energy Levels Form. (n.d.). https://physics.nist.gov/PhysRefData/ASD/levels_form.html